**Old Dominion University**
## ODU Digital Commons

Chemistry & Biochemistry Faculty Publications

Chemistry & Biochemistry

2015

# Characterization and Photodegradation of Dissolved Organic Matter (DOM) From a Tropical Lake and Its Dominant Primary Producer, the cyanobacteria Microcystis aeruginosa

Thais B. Bittar

Aron Stubbins

Armando A. H. Vieira

Kenneth Mopper
*Old Dominion University*, kmopper@odu.edu

Follow this and additional works at: https://digitalcommons.odu.edu/chemistry_fac_pubs

Part of the Chemistry Commons, Fresh Water Studies Commons, and the Oceanography Commons

CrossMark

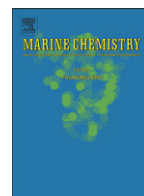# Characterization and photodegradation of dissolved organic matter (DOM) from a tropical lake and its dominant primary producer, the cyanobacteria *Microcystis aeruginosa*

Thais B. Bittar [a,*], Aron Stubbins [a], Armando A.H. Vieira [b], Kenneth Mopper [c]

[a] *Skidaway Institute of Oceanography, Marine Sciences Department, University of Georgia, 10 Ocean Science Circle, Savannah, GA 31411, USA*
[b] *Laboratory of Phycology, Department of Botany, Federal University of São Carlos, Via Washington Luis, km 235, São Carlos, São Paulo 13565-905, Brazil*
[c] *Department of Chemistry and Biochemistry, Old Dominion University, 4541 Hampton Boulevard, Norfolk, VA 23529, USA*

## ARTICLE INFO

## ABSTRACT

This study investigates optical and high-resolution molecular signatures and photochemical degradation of DOM from the Barra Bonita Reservoir (BB-DOM), a tropical eutrophic lake, as well as from its dominant phytoplankton species, the cyanobacteria *Microcystis aeruginosa* (*Microcystis*-DOM). Consistent with a predominantly autotrophic source, BB-DOM and *Microcystis*-DOM exhibited high protein-like fluorescence and contained a large number of aliphatics. *Microcystis*-DOM was enriched in peptide-like formulae, while BB-DOM had higher chromophoric and fluorescent DOM (CDOM and FDOM) and was enriched in moderately unsaturated formulae, indicating additions of terrigenous DOM and/or in situ processing of autochthonous material in the lake. Consistent with its higher CDOM content, BB-DOM was more photoreactive than *Microcystis*-DOM. For both types of DOM, photodegradation resulted in loss of CDOM, FDOM, moderately unsaturated structures, high O/C and low H/C formulae, and preservation of aliphatics. The majority of photoproducts of 0.5 d irradiation were subsequently removed by day 7, and photoproducts represented a minor fraction of the photo-irradiated DOM. For BB-DOM, molecular formula photolability increased with increasing aromaticity index values, while for *Microcystis*-DOM, molecular formula photolability increased with molecular mass. Photodegradation increased the proportion of molecular formulae containing N (CHO + N) in BB-DOM, while the molecular mass and the proportion of CHO + N formulae decreased upon photo-irradiation of *Microcystis*-DOM. In concert, these molecular shifts due to photodegradation decreased the diversity of and increased the similarity between BB-DOM and *Microcystis*-DOM, suggesting the selective pressure exerted by photochemistry selects for the survival of similar compounds in both samples.

© 2015 Elsevier B.V. All rights reserved.

## 1. Introduction

Photochemical degradation is one of the most important pathways of removal and transformation of dissolved organic matter (DOM) in aquatic systems (Mopper et al., 2015). Complete photooxidation of dissolved organic carbon (DOC) to inorganic forms ($CO_2$, CO) and photochemically-mediated alterations in DOM composition play significant roles in global C-cycling (Mopper et al., 1991; Stubbins et al., 2011). Optical, elemental and structural changes in DOM caused by light exposure have several implications for processes in the water column. For instance, exposure to sunlight, particularly ultra-violet (UV) radiation, can affect chemical composition (Helms et al., 2014; Minor et al., 2007) and biological availability of DOM, increasing or decreasing biodegradation (Moran et al., 2000; Stedmon and Markager, 2005; Tranvik and Bertilsson, 2001; Tranvik et al., 2000). UV exposure also causes loss of color (i.e., photobleaching) (Helms et al., 2013; Stubbins et al., 2012), increasing light penetration depths and the exposure of microorganisms to photosynthetically active radiation and harmful UV radiation, which affect both autotrophic and heterotrophic metabolism (Moran and Zepp, 1997; Vodacek et al., 1997; Walsh et al., 2003).

Carbon fluxes in freshwater ecosystems play an important role in global biogeochemical cycles (Aufdenkampe et al., 2011; Battin et al., 2009; Cole et al., 2007) and DOC concentration is one of the parameters used to define the trophic status of lakes (Williamson et al., 1999). In

natural lakes and man-made reservoirs, DOM is comprised of a mixture of products from indigenous phytoplankton primary productivity (autochthonous DOM), the surrounding watershed (terrigenous DOM) (Williamson et al., 1999), and the biotic and abiotic reworking of this DOM (Bittar et al., 2015). Generally, autochthonous DOM is more bio-labile, and less chromophoric and photo-labile, while terrigenous DOM is less bio-labile, and more chromophoric and photo-labile (Benner and Kaiser, 2011).

High resolution Fourier transform ion cyclotron resonance mass spectrometry (FTICR-MS) brings a major fraction of DOM into our analytical window, providing high accuracy molecular-level information regarding elemental and inferred structural composition that can be related to source (Dittmar and Stubbins, 2014; Kujawinski, 2002) and photochemical transformations of DOM (Gonsior et al., 2009; Kujawinski et al., 2004; Stubbins et al., 2010). The majority of DOM photodegradation studies from lakes are from temperate regions (Anesio and Granéli, 2003; Bertilsson and Tranvik, 2000; Boreen et al., 2008). There are few studies addressing the photochemical effects on DOM in tropical lakes, which are subject to intense solar radiation and warm temperatures throughout the year, favoring both high phytoplankton productivity and DOM photodegradation. The extent to which radiation-induced mechanisms in aquatic systems can be extrapolated from the temperate regions to the tropics is not clear (Lewis, 2000).

The Barra Bonita Reservoir (22°29′ S, 48°34′ W) is one of six cascade, man-made river-reservoirs created for power generation by constructing dams across the Tietê River in São Paulo State, one of the most populous areas of Brazil. The reservoir is located downstream from the confluence between the Tietê and the Piracicaba rivers, where the hydrology regime transitions from lotic to lentic (Tundisi et al., 2008). Seasonal patterns consist of a wet season (December through February) and a dry season (May to August), with only moderate variations in water temperature throughout the year (20 to 30 °C) (Dellamano-Oliveira et al., 2008). The reservoir is a eutrophic (i.e., nutrient-rich) and polymictic (i.e., thermally unstratified) tropical ecosystem, that has undergone eutrophication as a result of urban, agricultural and industrial development in the State of São Paulo (Tundisi et al., 2008). Increasing eutrophication of freshwater environments results in higher growth of cyanobacteria, such as *Microcystis* spp., *Anabaena* spp., and *Pseudo anabaena* spp. (Paerl and Huisman, 2008; Tien et al., 2002). Among these, those belonging to the genus *Microcystis* are of particular interest, as they often dominate massive and potentially toxic blooms in fresh and brackish waters around the world (Sivonen and Jones, 1999), producing significant amounts of DOM. While extensive research has focused upon *Microcystis* toxicity, the fate of DOM produced by this species is not well known (Paerl and Otten, 2013). In the Barra Bonita Reservoir, the most abundant species of phytoplankton is *M. aeruginosa*, which is present primarily as free cells (Calijuri et al., 2002; Dellamano-Oliveira et al., 2008). High tolerance to light stress, buoyancy regulation and low edibility are competitive advantages of *M. aeruginosa* (Brookes and Granf, 2001; Kluijver et al., 2012; Liu et al., 2004), which, combined with warm temperatures and light- and nutrient-replete conditions, lead to dominance of this species in the Barra Bonita Reservoir throughout the year (Dellamano-Oliveira et al., 2008). Consequently, *M. aeruginosa* is an important source of autochthonous DOM in the reservoir during both wet and dry seasons (Dellamano-Oliveira et al., 2008; Vieira et al., 2013). Terrigenous DOM, on the other hand, originates from watershed runoff and riverine input, particularly in the wet season. The catchment area is predominantly agricultural, interspersed with small industrial and urban areas. Watershed runoff is also the cause of high inflows of inorganic N and P, mainly of agricultural origin (Tundisi et al., 2008), which favors phytoplankton growth and release of DOM (Vieira et al., 2013; Welch and Lindell, 1992).

The goals of this study were, firstly, to characterize and compare the optical and molecular signatures of the DOM from the Barra Bonita Reservoir (BB-DOM) and from its dominant primary producer (laboratory cultured *Microcystis*; *Microcystis*-DOM). Secondly, the effects of photodegradation upon BB- and *Microcystis*-DOM were assessed in laboratory-controlled UVB irradiation experiments. DOM was characterized and the photochemically-mediated alterations were identified using bulk (DOC concentration), optical (chromophoric and fluorescent properties) and molecular-level (FTICR-MS) analyses. In addition, given that the DOM in the reservoir had undergone some degree of photodegradation by being exposed to full sunlight prior to our sampling, we anticipated that this sample would be more likely composed of photodegraded *Microcystis*-DOM than of unaltered *Microcystis* exudates. In order to test this hypothesis, we assessed whether the FTICR-MS profile of the DOM from the reservoir was more similar to that of UVB-exposed *Microcystis*-DOM than to the non-irradiated sample.

## 2. Materials and methods

### 2.1. Barra Bonita DOM (BB-DOM) sampling

Samples were collected from the Barra Bonita Reservoir in an 800 m wide section of the reservoir, ~6 km upstream of the hydroelectric dam and ~20 km downstream from the point where the Piracicaba River joins the Tietê River (Fig. 1). Water depth was ~20 m at the sampling site. A depth-integrated 20 L water sample was collected on January 28, 2008, using a Niskin sampler and sterile (autoclaved) collection bottle and tubing. The depth integrated sample was generated by combining equal volumes of water collected from 0, 1, 3, 7, 10, 15 and 18 m. On the sampling day, a massive phytoplankton bloom was visible and microscopic analysis showed that the bloom was dominated by free cells of *Microcystis* sp. UVB radiation was measured at the sampling site using a portable radiometer (EPP 2000, StellarNet) during daytime on January 22, 2008, with maximum intensity of 2.7 W m$^{-2}$ (Fig. S1).

The 20 L water sample was returned to the laboratory within 2 h and filtered through pre-combusted 1.2 μm pore size filters (GF/C, Whatman) to remove large particles. The <1.2 μm fraction was subsequently filtered using a tangential flow filtration system through a sterile 0.2 μm hollow fiber polysulfone cartridge (QuixStand Systems, GE) under low pressure (<5 psi). A subset of this filtrate containing the DOM (<0.2 μm) was frozen at −20 °C and shipped in the dark to Old Dominion University for the irradiation experiments. The filtration system was pre-washed with 5% NaClO and rinsed thoroughly with ultrapure deionized water (MilliQ, Millipore). Total organic carbon concentration measured in the ultrapure water after running through the filtration unit as an operational blank was <1 μM-C, which is below the minimum detection limit reported for DOC analysis using a Shimadzu high temperature combustion system (e.g., 2.8 ± 0.3 μM-C) (Stubbins and Dittmar, 2012).

### 2.2. M. aeruginosa DOM (Microcystis-DOM)

Axenic (bacteria-free) cultures of a *M. aeruginosa* strain isolated from the Barra Bonita Reservoir were used to obtain Microcystis-derived DOM. The strain is maintained in axenic conditions in the Culture Collection of Microalgae at the Botany Department, Federal University of São Carlos (World Data Center for Microorganisms No. 835). Axenic *M. aeruginosa* was cultured in batch mode in sterile (autoclaved) pH 7 Artificial Seawater McLachlan (ASM-1) medium containing inorganic nitrogen (NaNO$_3$, 2 mM-N) and phosphorus (K$_2$HPO$_4$ and Na$_2$HPO$_4$, 0.2 mM-P) in concentrations similar to that of the Barra Bonita Reservoir water (Dellamano-Oliveira et al., 2008; Gorham et al., 1964). In spite of the word seawater in the ASM acronym, this medium does not contain NaCl. DOC concentration of the medium was <10 μM-C prior to addition of *M. aeruginosa*. Cultures were lightly stirred and maintained in a temperature-controlled room (23 ± 1 °C) under a light:dark cycle of 12:12 h and light intensity of 32.7 W m$^{-2}$ (40 W fluorescent tubes, Philips TLT 40W/75 Extra Day Light). *M. aeruginosa*
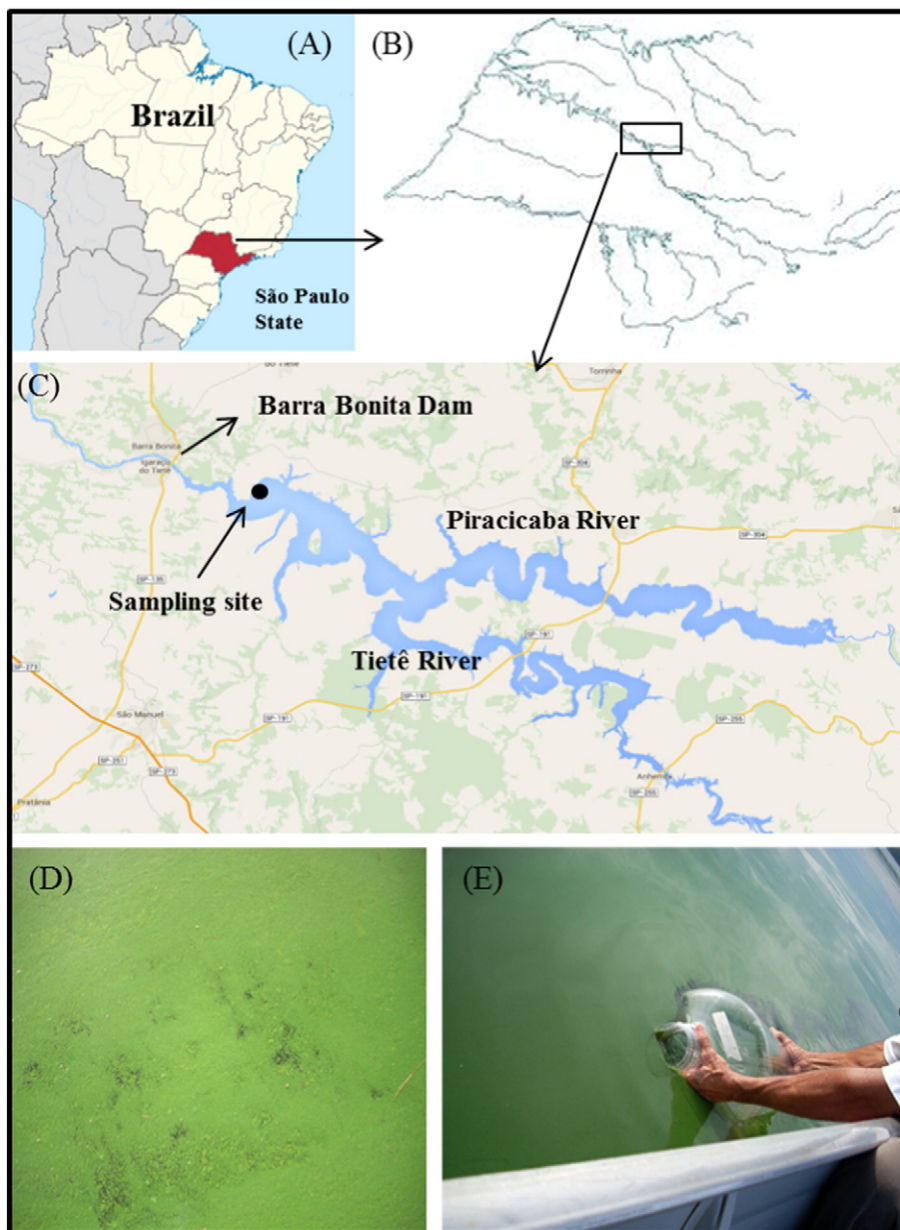
**Fig. 1.** Location of the Barra Bonita Reservoir, Tietê River and Piracicaba River and this study's sampling site (A, B, C) and a bloom of *Microcystis aeruginosa* in the reservoir (D, E). Sources: (A) Wikimedia Commons, http://pt.wikipedia.org/wiki/S%C3%A3o_Paulo, (B) Google maps, (C) http://www.brazilinvestmentguide.com/state-guides/sao-paulo/ (C, D), personal records.

growth rates were calculated from in vivo chlorophyll-a fluorescence using a Turner 10-AU fluorometer calibrated with chlorophyll-a standards (Sigma Chemical Co.). *M. aeruginosa* cultures reached the late exponential/early stationary growth phase in 30 d (data not shown), at which point the cells were removed by filtration through pre-combusted 1.2 μm pore size filters (GF/C, Whatman). DOM released by the cells that accumulated in the batch cultures was collected by tangential flow filtration through a sterile 0.2 μm pore size polypropylene cassette module (Pellicon Millipore) under low pressure (≤5 psi). Cleaning and handling of filtration apparatus were performed as described above for BB-DOM.

### 2.3. Simulated UVB irradiation

Prior to the irradiation experiments, the DOM samples were thawed and filtered once again through acid-washed, sterile (autoclaved) 0.22 μm pore size polycarbonate membrane filters (GTTP Isopore, Millipore) to remove any particles that could have formed during freezing. All glassware were previously autoclaved and combusted, and filtrations and handling of samples were performed in a sterile flow hood; the hood itself was sterilized with 70% ethanol solution and exposed to germicide UV bulbs for 1 h. In the sterile hood, DOM samples were transferred to 250 mL, pre-combusted quartz flasks and irradiated for 0, 0.5, 1, 3 and 7 d in a chamber equipped with 4 UVB bulbs (275 to 315 nm, TL40W-12-RS Philips) kept at 20 °C ($\pm 1$ °C). The UVB intensity reaching the flasks was 2.7 W m$^{-2}$ in order to simulate UVB levels at the surface of the Barra Bonita Reservoir. In these experiments, UVB exposure for 0.5 d and 7 d was equivalent to 1 d and 14 d, respectively, of exposure to natural UVB at the surface of the reservoir, assuming a 12:12 h light:dark cycle. Due to a limited volume of samples, particularly BB-DOM, that could be transported from Brazil to the lab at Old Dominion University, typical dark controls were not run in these experiments. While this is

not the ideal setup, great care was taken to avoid contamination of the DOM samples with bacteria, i.e., samples were filter-sterilized twice and materials that came in contact with the samples were pre-combusted (500 °C, overnight) and/or autoclaved. In addition, the UVB radiation used in these time-series experiments is likely to inhibit bacterial growth and activity during these relatively short term experiments.

## 2.4. DOM characterization

Irradiated samples were not filtered prior to analyses for DOM characterization. The absence of visible particles and the low absorbance coefficients of CDOM at wavelengths longer than 500 nm indicated that photo-flocculation did not occur during these irradiations. In addition, photo-flocculation has been shown to take place in DOM samples with levels of terrestrial material and iron significantly greater than those in this study (Helms et al., 2013). The lack of particles detectable by eye or via spectrophotometry provided further evidence that microbial growth did not occur during the irradiations.

Bulk concentrations of DOM are reported as non-purgeable DOC and were obtained by high temperature combustion (680 °C) and non-dispersive infrared detection (NDIR) using a total organic carbon analyzer (TOC-Vcph, Shimadzu). At least triplicate sample injections were made for each sample, with a standard deviation of 0.2 μM-C. The instrument was calibrated with standard solutions of potassium hydrogen phthalate from 0.1 to 1 mM-C (Stubbins and Dittmar, 2012).

Chromophoric (absorbance) and fluorescent DOM (CDOM and FDOM) were characterized. Ultrapure water was used as blanks for CDOM and FDOM analyses. Absorbance spectra of the ASM-1 medium represented 15% of the absorbance coefficient at 254 nm obtained for non-irradiated Microcystis-DOM. The absorbance spectrum of the medium was not used as a blank for CDOM analysis because the medium composition changed during the 30 d of Microcystis culturing, i.e., the light-absorbing constituents (mainly nitrate) were consumed by Microcystis. Measurements of total dissolved nitrogen (TDN) on day 0 and day 30 of Microcystis culturing showed that TDN was reduced to 10% of its initial concentration. Therefore, nitrate concentrations and the background absorbance of the medium was likely negligible after 30-d. For each DOM sample, duplicate absorption spectra of CDOM from 250 to 800 nm at 1 nm intervals were obtained using a UV−visible diode array spectrophotometer (Agilent 8453) and a 5 cm acid-washed quartz cuvette. Spectra were corrected for light scatter by subtracting absorption from 750 to 800 nm, and Napierian light absorption coefficients were calculated ($a\,m^{-1}$) (Green and Blough, 1994). First and second derivative spectra were determined using linear regression over sliding 21 nm intervals. The second derivative spectra were used to accurately determine peaks that appeared as shoulders in the absorption coefficient spectra (Helms et al., 2013; Loiselle et al., 2009). Specific UV absorbance ($SUVA_{254}$) was calculated using the decadic light absorption coefficient at 254 nm ($m^{-1}$) normalized to DOC (mg-C $L^{-1}$) and used as a proxy for aromaticity (Weishaar et al., 2003).

Excitation–emission matrix (EEM) spectra for analysis of FDOM were determined using a spectrofluorometer (Fluoromax 2) and a 1 cm acid-washed quartz cuvette (Spencer et al., 2007). Each EEM was comprised of 37 emission spectra from 300 to 500 nm in 1 nm intervals, at excitation from 240 to 420 nm in 5 nm intervals and both emission and excitation slits were set to 5 nm. Blank EEMs were collected from ultrapure water and subtracted from sample EEMs. EEMs were corrected using instrument-specific excitation (xcorrect) and emission (mcorrect) correction files, and for inner-filter effects using Matlab version 7.14 (Cory et al., 2010). Corrected EEMs were normalized to Raman units and FDOM components were identified by parallel factor analysis (PARAFAC). A PARAFAC model was developed using EEMs for 122 samples from Microcystis-DOM and BB-DOM using the DOM Fluor toolbox in Matlab version 7.14 (Stedmon and Bro, 2008). The model was validated using random split-half analysis and the number of components was determined by visual examination of the residuals from models

with gradually increasing number of components. Intensities of each component were calculated as the maximum fluorescent intensity of each component, i.e., using maxval values (Stedmon and Bro, 2008).

Three samples from each time series experiment (BB-DOM and Microcystis-DOM) were selected for analysis by negative mode electrospray ionization (ESI, Apollo II) Fourier transform ion cyclotron resonance mass spectrometry (FTICR-MS) (Bruker Daltonics 12 Tesla Apex Qe), at the College of Sciences Major Instrumentation Cluster (COSMIC), Old Dominion University, Virginia, U.S.A. (Sleighter et al., 2008). The samples analyzed by FTICR-MS from each DOM were: 0 d (non-irradiated), 0.5 d and 7 d UVB irradiated samples. Whole samples (unfractionated) were prepared by dilution (50:50 v/v) with ultrapure methanol plus 0.1% ammonium hydroxide (pH 8) and infusion rates into the ESI ion source were 120 μL $h^{-1}$. Ion accumulation time in the hexapole was 1 s and 300 transients were collected with a 4 M word time domain (Chen et al., 2011). Mass spectra of peaks with signal to noise ratio > 4 ranged from 200 to 800 m/z and were internally calibrated using data lists of fatty acids and a list of peaks common to all samples (Sleighter et al., 2008). Molecular formula assignment was performed using a toolbox in Matlab version 7.14, based on exact masses (±800 ppb) and published rules (Spencer et al., 2014; Stubbins et al., 2010) for atomic composition as follows: C ≤ 50; H/C ≥ 0.3; O/C ≤ 1; N ≤ 4; S ≤ 2; and P ≤ 1. The relatively high number of N and S was allowed in the molecular assignment because DOM from Microcystis axenic cultures is likely to contain unaltered amino acids and peptides which may have multiple N and S atoms. Total number of peaks were 1581, 1634 and 1130 for BB-DOM 0 d, 0.5 d and 7 d, respectively; and 1280, 1404 and 1180 for Microcystis-DOM 0 d, 0.5 d and 7 d, respectively. Number of single-charged and single-formula assigned peaks were 436, 426 and 150 for BB-DOM 0 d, 0.5 d and 7 d, respectively, and 309, 328 and 151, for Microcystis-DOM 0 d, 0.5 d and 7 d, respectively. Only single-charged peaks and unambiguously assigned molecular formulae were included in the final list of compounds comprising each DOM sample. The trends observed in total peaks and single-formula assigned peaks were similar, with lesser peak diversity in the samples irradiated longer.

Assigned formulae were categorized as CHO-only: only C, H and O in the molecular formula; CHO + N: formulae with N, regardless of the presence of P or S (CHON, CHONS, CHONP and CHONSP); and CHO + P/S: formulae with either P or S, but without N (CHOP, CHOS and CHOPS). Peaks were also categorized into likely structural groups, based on double bond equivalents (DBE) (Mclafferty and Turecek, 1993), modified aromaticity index ($AI_{mod} = [(1 + \#C − 0.5 * \#O − \#S − 0.5 * \#H) / (\#C − 0.5 * \#O − \#S − \#N − \#P)]$, where #C = number of carbon atoms, #O = number of oxygen atoms, #S = number of sulfur atoms, #H = number of hydrogen, #N = number of nitrogen atoms and #P = number of phosphorus atoms in a given formula (Koch and Dittmar, 2006), the elemental ratios of H/C and O/C, and the number of N in the formula. The molecular criteria used to define the structural groups in this study were similar to those previously described by Stubbins et al. (2014). Structural groups were aromatics ($AI_{mod} ≥ 0.5$), moderately unsaturated structures ($AI_{mod} < 0.5$, O/C < 0.9 and H/C < 1.5), unsaturated aliphatics (N = 0, O/C < 0.9 and 2 ≤ H/C ≥ 1.5), peptide-like (N > 0, O/C < 0.9, H/C ≥ 1.5), saturated fatty acids (N = 0, O/C < 0.9 and H/C > 2) and sugars (O/C ≥ 0.9).

## 2.5. Interpretation of FTICR-MS data within time-series comparisons

A comparison of FTICR-MS derived formulae present at 0 d, 0.5 d and 7 d within each DOM time-series experiment revealed six photoreactivity-defined pools of DOM: (1) Highly photolabile (present in 0 d, absent in 0.5 d, absent from 7 d); (2) Moderately photolabile (present in 0 d, present in 0.5 d, absent from 7 d); (3) Photoresistant (present in 0 d, present in 0.5 d, present in 7 d); (4) Photolabile photo-products (absent from 0 d, present in 0.5 d, absent from 7 d); (5) Photoresistant photoproducts (absent from 0 d, present in 0.5 d,

present in 7 d); (6) "Long-term" photoproducts (absent from 0 d, absent from 0.5 d, present in 7 d).

### 2.6. Statistical analyses

Changes in DOC concentration, SUVA$_{254}$ and fluorescence intensity of PARAFAC-derived FDOM components over the irradiation time-series were fit with the following three-parameter decay function: $y_t = y_0 \exp^{(-\lambda t)} + b$, where $y_0$ = y-axis value at time 0 (0 d), representing the photoreactive DOM fraction at time 0; $y_t$ = modeled y-axis value at a given time; $\lambda$ = decay constant, or rate of decay; $t$ = time (d); $b$ = y-axis projected value at time equals infinity, representing the non-reactive DOM fraction; and exp = the base of the natural logarithm, using Sigma Plot v. 12.0 from Systat Software Inc. Decay constants ($\lambda$, d$^{-1}$) and standard errors are presented.

The Jaccard similarity index (JSI) (Jaccard, 1912) ranging from 0 to 1, where 0 = dissimilar and 1 = identical, was calculated as JSI = # of formulae common to both samples / (# formulae unique to BB-DOM + # formulae unique to *Microcystis*-DOM + # formulae common to both samples), to evaluate similarity between BB-DOM and *Microcystis*-DOM, before and after 0.5 d and 7 d irradiations. Frequency distributions of molecular formulae are presented for the variables AI$_{mod}$ and molecular mass (Da) as number of formulae per class intervals (bins). The bins for each variable were mutually exclusive and defined arbitrarily as 0.1 intervals for AI$_{mod}$ and 200 Da intervals for molecular mass. Unpaired, non-parametric Mann–Whitney tests were used to compare molecular formulae composition of BB- and *Microcystis*-DOM at a given time point, and an unpaired non-parametric ANOVA (Kruskal–Wallis) test was used to compare molecular mass and AI$_{mod}$ between time points for each DOM type.

## 3. Results

### 3.1. Characterization of BB-DOM and Microcystis-DOM before irradiation (0 d)

DOC concentration, and absolute absorbance and fluorescence intensities were greater for BB-DOM than for *Microcystis*-DOM (Table 1, Figs. 2A–B and 3). After DOC-normalization, absorbance (SUVA$_{254}$) and fluorescence remained greater for BB-DOM than for *Microcystis*-DOM (Table 1, Figs. 3 and 4). The second derivative spectra revealed four CDOM peaks in BB-DOM, at 290 nm ($a$290), ~315 nm ($a$315), 362 nm ($a$362) and 430 nm ($a$430); and four CDOM peaks in *Microcystis*-DOM, at 282 nm ($a$282), ~310 nm ($a$310), 350 nm ($a$350) and 382 nm ($a$382) (Fig. 2C–D, solid arrows). The PARAFAC model identified 3 components (Fig. S2), which are described using classical nomenclature (Coble, 1996) as peak T (bio-labile, protein-like, with Ex/Em = 275/338); peak M (semi-bio-labile, marine or autochthonous humic-like, with Ex/Em = 315/388); and peak C + A (bio-refractory, terrigenous humic-like, with Ex/Em = 350/451 and 245/451, respectively). BB-

DOM had similar proportion of fluorescence of peaks T, C + A and M, while peak T accounted for just over half of *Microcystis*-DOM fluorescence (Table 1, Fig. 4).

FTICR-MS showed differences in the chemical composition of BB- and *Microcystis*-DOM at 0 d (non-irradiated) (Table 2). BB-DOM molecular mass was 38 Da lower than *Microcystis*-DOM (Mann–Whitney, p < 0.0001). BB-DOM was dominated by CHO-only formulae (81%) and moderately unsaturated structures (56%), while *Microcystis*-DOM was mainly comprised of N-containing formulae (CHO + N, 55%) and the most common structures were moderately unsaturated (32%) and peptide-like formulae (30%). Unsaturated aliphatics represented 30% and 24%, in BB- and *Microcystis*-DOM, respectively. BB- and *Microcystis*-DOM had 105 formulae in common before irradiation (0 d), and the Jaccard similarity index (JSI) between the two types of DOM at 0 d was 0.16 (Table 2). JSI calculated for each elemental and structural class of FTICR-MS formulae showed that saturated fatty acids (0.71), unsaturated aliphatics (0.39), and CHO + P/S (0.29) exhibited the highest similarity between BB- and *Microcystis*-DOM (Table 2).

### 3.2. UVB-degradation of BB-DOM and Microcystis-DOM

In BB-DOM, UVB irradiation caused a linear decrease in CDOM absorbance over time, with greater bleaching at shorter wavelengths (Fig. 2A). For *Microcystis*-DOM, UVB exposure caused a non-linear decrease in CDOM absorbance from 250 nm to 335 nm over time, and an increase in absorbance from 335 nm to 500 nm within 0.5 d followed by a decrease at all wavelengths from 0.5 d to 7 d of exposure (Fig. 2B). UVB exposure caused qualitative shifts in CDOM, as shown by the second derivative CDOM absorption spectra. In BB-DOM, peak $a$290 shifted by ~10 nm towards shorter wavelengths ($a$280), peak $a$315 did not shift significantly and peak $a$362 shifted 10 nm towards longer wavelengths ($a$372) over time, while peak $a$430 disappeared within 0.5 d (Fig. 2C). In *Microcystis*-DOM, CDOM peaks $a$282, $a$350 and $a$382 shifted towards shorter wavelengths by 10 nm ($a$272), 30 nm ($a$320) and 5 nm ($a$377), respectively, while peak $a$310 disappeared within 0.5 d (Fig. 2D).

Within the first 0.5 d of UVB exposure, BB-DOM absorbance at 254 (CDOM $a$254) was reduced by 41% and at the end of the experimental time-series (7 d) $a$254 was reduced by 80% (Fig. 3A). For *Microcystis*-DOM, $a$254 increased slightly within 0.5 d and was reduced by 63% at 7 d (Fig. 3B). Photochemical loss of DOC in BB-DOM was measurable from 0.5 d to 7 d of UVB exposure, while DOC decay in *Microcystis*-DOM was minimal until 1 d of exposure, but measurable between 1 d and 7 d (Fig. 3). DOC decay constant values ($\lambda$, d$^{-1}$) over the irradiation time-series were similar for both types of DOM, while $\lambda$ of SUVA$_{254}$ were significantly greater for BB-DOM than for *Microcystis*-DOM (Fig. 3). Total DOC loss over the time-series was 32% and 19% in BB-DOM and *Microcystis*-DOM, respectively. The more efficient removal of CDOM relative to bulk DOC resulted in reductions in SUVA$_{254}$ by 74% and 54% for BB- and *Microcystis*-DOM, respectively.

For the first 0.5 d of exposure, DOC-normalized fluorescence intensity of peaks T, M and C + A in BB-DOM decreased, respectively, by 65%, 58% and 26%, while in *Microcystis*-DOM the decrease was 91%, 87% and 49%, respectively (Fig. 4). $\lambda$ of DOC-normalized fluorescence intensity of peaks T and M over the experimental time-series were smaller in BB-DOM than in *Microcystis*-DOM (Fig. 4A–D), while $\lambda$ of peak C + A were the smallest among FDOM components, and similar between the two types of DOM (Fig. 4E–F).

Based on FTICR-MS data, shifts occurring within 0.5 d of irradiation were evident in BB-DOM when relative peak intensity, rather than number of formulae (i.e., presence/absence), of each structural class was considered (Table 2). Shifts in the number of molecular formulae, on the other hand, were more dramatic in 7 d-irradiated samples than in 0.5 d-irradiated samples, relative to non-irradiated samples (0 d) for both DOM types (Table 2, Fig. 5). At the end of the experimental time series (7 d), the total number of formulae was reduced by 65% in BB- and 51% in *Microcystis*-DOM. The variation in molecular mass (Da) was not

**Table 1**
DOC concentrations, CDOM ($a$254 and SUVA$_{254}$) and FDOM absolute, relative (in brackets, %) and DOC-normalized fluorescence intensity measurements of DOM from the Barra Bonita Reservoir (BB-DOM) and from axenic cultures of *Microcystis aeruginosa* (*Microcystis*-DOM) before irradiation (0 d).

|  | BB-DOM | *Microcystis*-DOM |
|---|---|---|
| DOC (mM-C) | 1.60 | 0.97 |
| $a$254 (m$^{-1}$) | 93 | 17 |
| SUVA$_{254}$ (mg C L$^{-1}$ m$^{-1}$) | 2.10 | 0.64 |
| FDOM total (r.u.; %) | 4.7 (100) | 1.9 (100) |
| Peak T | 1.6 (33) | 1.0 (51) |
| Peak M | 1.4 (29) | 0.3 (17) |
| Peak C + A | 1.8 (38) | 0.6 (32) |
| FDOM total (r.u. mM-C$^{-1}$) | 3.0 | 2.0 |
| Peak T | 1.0 | 1.0 |
| Peak M | 0.9 | 0.3 |
| Peak C + A | 1.1 | 0.6 |
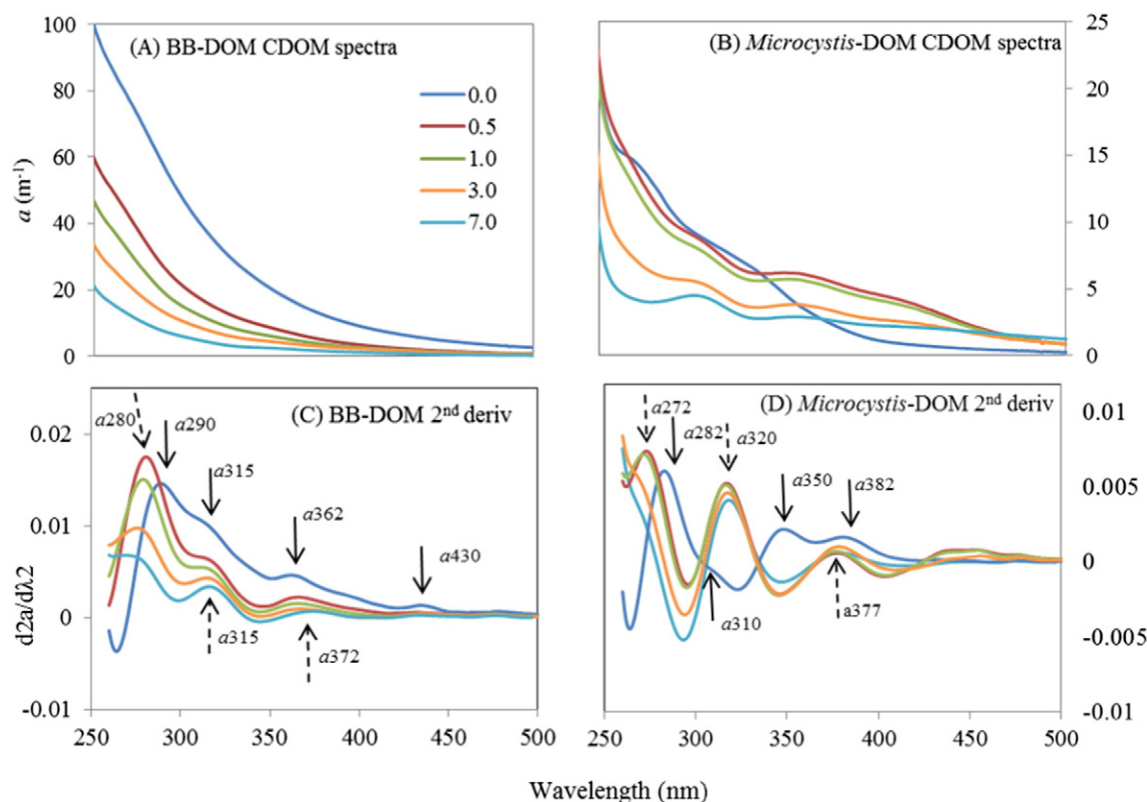
**Fig. 2.** CDOM absorbance spectra (A, B) and second derivative CDOM absorption spectra (C, D) of non-irradiated (0 d) and UVB irradiated (0.5, 1, 3, 7 d) DOM from the Barra Bonita Reservoir (A, C) and axenically-cultured *Microcystis* (B, D). Solid arrows and dashed arrows represent peaks and shoulders in the CDOM spectra of non-irradiated (0 d) and UVB irradiated DOM, respectively.

significant in BB-DOM over time of UVB exposure (ANOVA, p > 0.05), while in *Microcystis*-DOM, molecular mass decreased by 50 Da after 7 d (ANOVA, p < 0.0001) (Table 2). In BB-DOM, UVB exposure decreased the relative content of CHO-only formulae (81% to 59%), and caused a relative enrichment in CHO + N formulae (7% to 17%), while in *Microcystis*-DOM, UVB exposure resulted in relative increase in CHO-only (27% to 57%) and a decrease in CHO + N formulae (55% to 19%) at 7 d (Table 2). As a consequence of these opposite photochemically-mediated shifts, the elemental compositions and molecular masses of BB- and *Microcystis*-DOM were more similar to one another at 7 d than prior to irradiation (0 d), with CHO of 57–59%, CHO + N of 17–19% and a 15 Da difference in median molecular mass (Table 2). Structural changes caused by UVB irradiation were similar for both BB- and *Microcystis*-DOM, with preferential photochemical removal of moderately unsaturated structures, and photochemical enrichment of aliphatics (Table 2, Fig. 5). Photodegradation shifted both DOM types towards a less oxidized (lower O/C) and more saturated (higher H/C) state, particularly at 7 d of exposure (Fig. 5). In summation, the elemental, mass-related, structural and oxidation/saturation shifts over the irradiation time-series gradually increased the Jaccard similarity index (JSI) between BB-DOM and *Microcystis*-DOM from 0.16 at 0 d, to 0.19 at 0.5 d and 0.59 at 7 d (Table 3).

### 3.3. Photochemically produced compounds

Photoproducts accounted for a minor fraction of the total number of formulae in all irradiated samples: 15% in both 0.5 d and 7 d BB-DOM, and 17% and 32%, respectively, in 0.5 d and 7 d *Microcystis*-DOM. Photoproducts at the shortest irradiation time (0.5 d) were classified as photoresistant or photolabile depending on whether they were, respectively, present in or absent from the 7 d irradiated sample (see section Interpretation of FTICR-MS data within time-series comparisons for descriptions). The photoproducts of 0.5 d irradiation of BB-DOM were more photolabile than those of *Microcystis*-DOM. In BB-DOM, 65 formulae appeared within 0.5 d of exposure (photoproducts), of

which 50 (77%) were photolabile, and the other 15 (23%) were photoresistant (i.e., present at 7 d). For *Microcystis*-DOM, 55 photoproducts were detected at 0.5 d, 32 (58%) were photolabile and 23 (42%) were photoresistant until 7 d. For BB-DOM, the photoresistant photoproducts had O/C < 0.3 while most photolabile photoproducts had O/C spanning from 0.3 to 0.6 (Fig. 5E), suggesting continued photo-oxidation occurred from 0.5 d to 7 d. In *Microcystis*-DOM, most photoresistant photoproducts had H/C from 1.5 to 2, while photolabile photoproducts had H/C across the range from 1 to >2 (Fig. 5F). For both types of DOM, the majority of photoproducts had low $AI_{mod}$ values (<0.2) and molecular mass between 300 and 500 Da and, thus, no clear patterns of photolability of photoproducts were detected regarding aromaticity/degree of molecular conjugation or molecular mass (data not shown). "Long-term" photoproducts accounted for 7 formulae in the 7 d-irradiated BB-DOM and 26 formulae in the 7 d-irradiated *Microcystis*-DOM, and the majority of these had high H/C (Fig. 5E, F).

### 3.4. Photochemical lability gradient

The distribution in van Krevelen space of each photolability defined group (i.e., photoresistant, moderately- and highly photolabile, see section Interpretation of FTICR-MS data within time-series comparisons for descriptions) showed that the highly photolabile formulae had O/C spanning from 0.2 to 0.4 and H/C between 1.2 and 1.5 for BB- and *Microcystis*-DOM (Fig. 5A, B). In the moderately photolabile group these ranges were expanded to greater O/C (up to 0.55 in BB and to 0.9 in *Microcystis*) as well as greater H/C (up to 1.6 in BB and 1.9 in *Microcystis*) (Fig. 5A–D). Photoresistant compounds had mostly low O/C (<0.2) and/or high H/C (between 1.75 and 2.5) (Fig. 5A–F).

The frequency of distribution of formulae in each photolability-defined group for the variables $AI_{mod}$ (modified aromaticity index) and molecular mass (Da) is presented in Fig. 6. In BB-DOM, highly photolabile compounds had high values of $AI_{mod}$ (0.3 to 0.39), moderately photolabile had intermediate $AI_{mod}$ (0.1 to 0.29), and
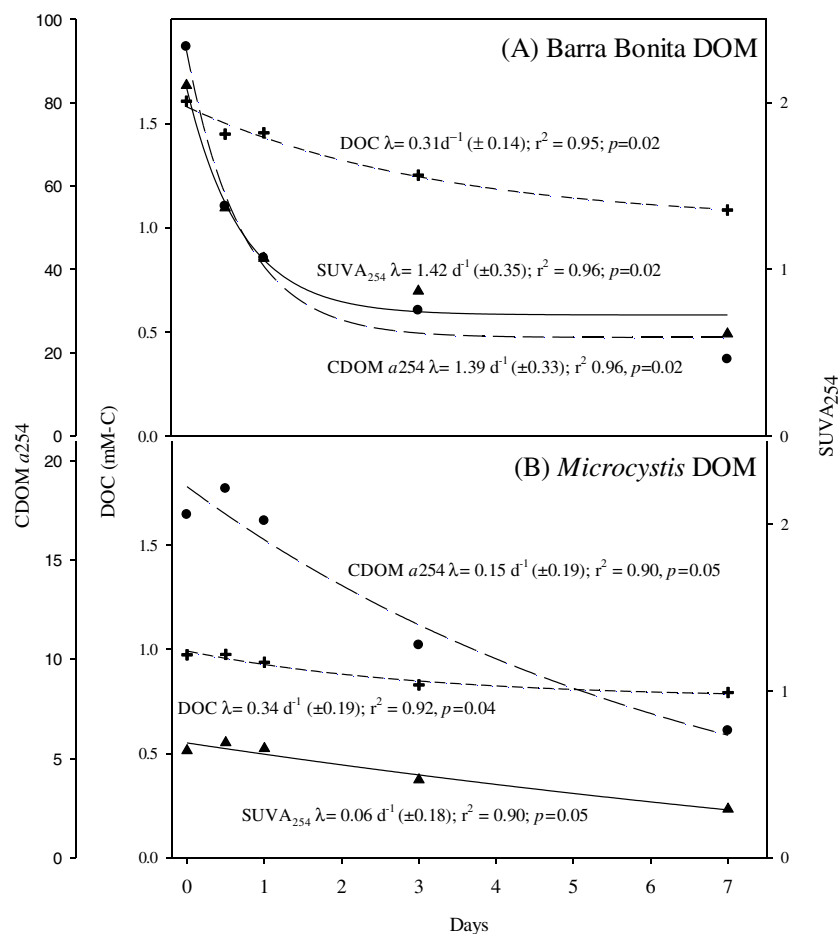
**Fig. 3.** Loss of dissolved organic carbon (DOC, mM-C, crosses, short-dashed lines), CDOM absorbance at 254 nm ($a254$, $m^{-1}$, circles, long-dashed lines) and specific UV absorbance (SUVA$_{254}$, mg C L$^{-1}$ m$^{-1}$, triangles, solid lines) over UVB irradiation time series of DOM from Barra Bonita Reservoir (A) and axenically-cultured *Microcystis* (B). Decay rates ($\lambda$, d$^{-1}$) ($\pm$standard error); adjusted $r^2$ and p value of modeled data are presented.

photoresistant compounds had the lowest AI$_{mod}$ ($\leq 0.1$) (Fig. 6A), indicating an association between photolability and the degree of molecular conjugation. There was no clear association between photolability and molecular mass in BB-DOM, since all three groups had frequency of distribution of formulae centered between 300 and 400 Da (Fig. 6B). These results are in agreement with the overall significant decrease in AI$_{mod}$ (ANOVA, p < 0.0001) and not significant change in molecular mass (ANOVA, p > 0.05) in BB-DOM over the UVB irradiation time-series (Table 2). In *Microcystis*-DOM, all three photolability-defined groups had AI$_{mod}$ < 0.1 (Fig. 6C) and, thus the relationship between photolability and molecular conjugation was less clear than for BB-DOM. Nonetheless, a number of moderately photolabile formulae with AI$_{mod}$ of 0.2–0.29 (33 formulae) and 0.4–0.49 (35 formulae) resulted in overall decrease in AI$_{mod}$ of *Microcystis*-DOM over the experimental time series (ANOVA, p = 0.005, Table 2). Highly and moderately photolabile *Microcystis*-DOM formulae had masses between 400 and 500 Da (Fig. 6D), while the photoresistant compounds were smaller (300 to 400 Da) (Fig. 6D), showing an association between photolability and molecular mass in *Microcystis*-DOM. Such association was reflected in a statistically significant 50 Da-decrease in molecular mass of *Microcystis*-DOM over the irradiation (ANOVA, p < 0.0001, Table 2).

## 4. Discussion

### 4.1. Signatures of BB-DOM and Microcystis-DOM

The exudation of DOM by live phytoplankton is a natural process influenced by physiological status, membrane permeability, and the

intracellular excess of specific compounds (Fogg, 1983; Mague et al., 1980), among other factors. *Microcystis* is the dominant phytoplankton in Barra Bonita (Dellamano-Oliveira et al., 2008; Vieira et al., 2008), and thus is expected to contribute significantly with the autochthonous production of DOM in the reservoir. *Microcystis*-DOM is highly biolabile (Bittar et al., 2015), which implies high biological alteration and turnover rates of DOM in the environment (Vieira et al., 2013). Other sources of DOM also exist for Barra Bonita. Therefore, BB-DOM and *Microcystis*-DOM may exhibit quite distinct molecular features.

DOC production rates in laboratory cultures do not accurately reflect the amount of DOC released by natural populations of *Microcystis* in Barra Bonita, given that phytoplankton DOC production is influenced by growth conditions (Fogg, 1983). Therefore, the amount of BB-DOM that originates from *Microcystis* exudation could not be determined in this study. Optical and FTICR-MS provide information on DOM quality, including dominant sources and subsequent processing (Fellman et al., 2010; Dittmar and Stubbins, 2014). In this study, many characteristics of *Microcystis*-DOM were shared with BB-DOM. Given the non-quantitative character of these analyses, these similarities have to be interpreted with great care. For instance, 24% of the FTICR-MS formulae identified in BB-DOM had molecular features identical to axenic *Microcystis*-DOM (Table 2) and, unsaturated aliphatics and saturated fatty acids displayed high similarity indexes between BB- and *Microcystis*-DOM (0.39 and 0.71, respectively, Table 1), implying that *Microcystis* could be an important source of this material in the reservoir. However, identical molecular formulae can represent distinct isomers (i.e., completely distinct compounds, Sleighter and Hatcher, 2008) and the overlap between BB- and *Microcystis*-DOM does not rule out other
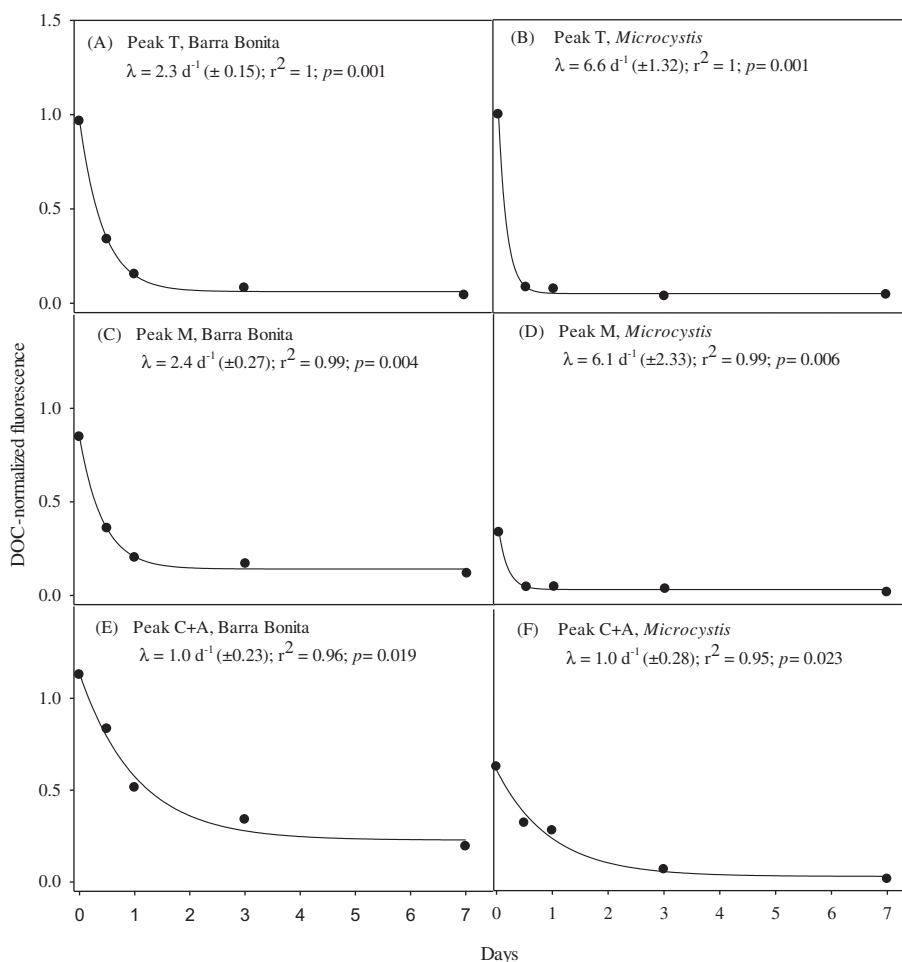
**Fig. 4.** Decay of DOC-normalized fluorescence intensity of peak T (A, B), peak M (C, D), and peak C + A (E, F) over UVB irradiation time series of DOM from Barra Bonita Reservoir (A, C, E) and axenically-cultured *Microcystis* (B, D, F). Decay rates ($\lambda$, $d^{-1}$) ($\pm$ standard error); adjusted $r^2$ and p value of modeled data are presented.

**Table 2**
Molecular formulae characterization of BB-DOM and *Microcystis*-DOM at each irradiation time (0 d, 0.5 d and 7 d), and common formulae ('Common 0 d') and Jaccard similarity index (JSI) of BB-DOM and *Microcystis*-DOM prior to irradiation (0 d). Number (#) of singly-assigned formulae, median of molecular mass (Da), median of modified aromaticity index ($AI_{mod}$), elemental composition (number of CHO-only, CHO + P/S and no N, and CHO + N formulae) and structural composition (number of formulae [#] and relative peak intensity [rel. int.]). Numbers in brackets are percentages (%).

| | | BB 0 d | BB 0.5 d | BB 7 d | *Microcystis* 0 d | *Microcystis* 0.5 d | *Microcystis* 7 d | Common 0 d | JSI |
|---|---|---|---|---|---|---|---|---|---|
| All | # | 436 | 426 | 150 | 309 | 328 | 151 | 105 | 0.16 |
| Molecular mass | Median | 365 | 362 | 368 | 403 | 413 | 353 | 326 | – |
| $AI_{mod}$ | Median | 0.19 | 0.18 | 0.09 | 0.13 | 0.10 | 0.05 | 0.07 | – |
| CHO | # (%) | 353 (81) | 351 (82) | 89 (59) | 82 (27) | 90 (27) | 86 (57) | 67 | 0.18 |
| | Rel. int. | 0.79 | 0.84 | 0.64 | 0.29 | 0.31 | 0.73 | | |
| CHO + P/S | # (%) | 53 (12) | 44 (10) | 36 (24) | 58 (19) | 72 (22) | 36 (24) | 26 | 0.29 |
| | Rel. int. | | 0.09 | 0.26 | 0.21 | 0.22 | 0.18 | | |
| CHO + N | # (%) | 30 (7) | 31 (7) | 25 (17) | 169 (55) | 166 (51) | 29 (19) | 12 | 0.06 |
| | Rel. int. | 0.06 | 0.06 | 0.10 | 0.51 | 0.47 | 0.09 | | |
| Aromatics | # (%) | 6 (1) | 11 (3) | 11 (7) | 19 (6) | 25 (8) | 8 (5) | 1 | 0.04 |
| | Rel. int. | 0.01 | 0.02 | 0.05 | 0.11 | 0.10 | 0.02 | | |
| Moderately unsaturated | # (%) | 246 (56) | 214 (50) | 32 (21) | 100 (32) | 97 (30) | 19 (13) | 19 | 0.06 |
| | Rel. int. | 0.41 | 0.29 | 0.13 | 0.26 | 0.24 | 0.09 | | |
| Unsaturated aliphatics | # (%) | 143 (33) | 165 (39) | 67 (45) | 73 (24) | 84 (26) | 76 (50) | 61 | 0.39 |
| | Rel. int. | 0.48 | 0.60 | 0.58 | 0.29 | 0.32 | 0.67 | | |
| Saturated fatty acids | # (%) | 23 (5) | 17 (4) | 23 (15) | 18 (6) | 25 (8) | 27 (18) | 17 | 0.71 |
| | Rel. int. | 0.06 | 0.04 | 0.16 | 0.03 | 0.06 | 0.12 | | |
| Peptide-like | # (%) | 16 (4) | 16 (4) | 13 (9) | 94 (30) | 93 (28) | 20 (13) | 7 | 0.07 |
| | Rel. int. | 0.04 | 0.04 | 0.06 | 0.28 | 0.26 | 0.10 | | |
| Sugars | # (%) | 2 (0) | 3 (1) | 4 (3) | 5 (2) | 4 (1) | 1 (1) | 0 | 0.00 |
| | Rel. int. | 0.00 | 0.00 | 0.02 | 0.03 | 0.03 | 0.00 | | |
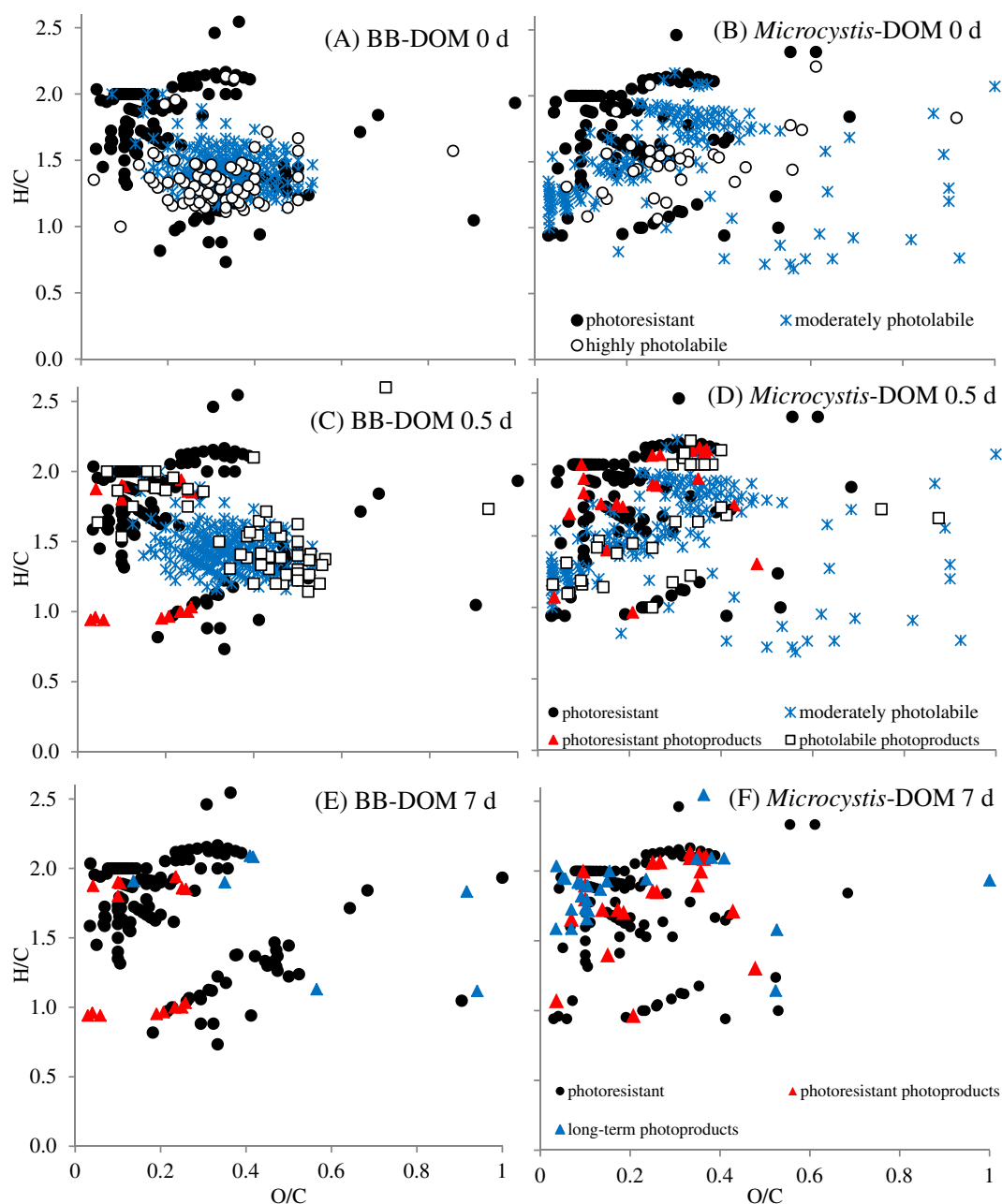
**Fig. 5.** Van Krevelen diagrams of FTICR-MS formulae in each photolability defined group: photoresistant (black dots), highly photolabile (white dots), moderately photolabile (blue crosses) that comprise samples at 0 d (non-irradiated) for BB-DOM (A) and *Microcystis*-DOM (B); photoresistant, moderately photolabile, photoresistant photoproducts (red triangles) and photolabile photoproducts (open squares) that comprise samples irradiated for 0.5 d for BB-DOM (C) and *Microcystis*-DOM (D); and photoresistant, photoresistant photoproducts and long-term photoproducts (blue triangles) that comprise samples irradiated for 7 d for BB-DOM (E) and *Microcystis*-DOM (F).

sources (e.g., other phytoplankton) for these formulae. Similarly, BB-DOM and *Microcystis*-DOM had similar DOC-normalized peak T, which may indicate that this component in the reservoir is strongly influenced

**Table 3**
Jaccard similarity index (JSI) between FTICR-MS singly-assigned molecular formulae in BB-DOM and *Microcystis*-DOM before (0 d) and after 0.5 d and 7 d of UVB irradiation.

|  | BB-DOM | BB-DOM | BB-DOM |
|---|---|---|---|
|  | 0 d | 0.5 d | 7 d |
| *Microcystis*-DOM 0 d | 0.16 | 0.17 | 0.23 |
| *Microcystis*-DOM 0.5 d | 0.18 | 0.19 | 0.27 |
| *Microcystis*-DOM 7 d | 0.24 | 0.26 | 0.59 |

by the continuous release of protein-like material by *Microcystis*. Furthermore, BB-FDOM had high relative intensity of peak T when compared to terrestrially-influenced waters (Cory et al., 2007), which may simply indicate that FDOM in the reservoir is highly influenced by phytoplankton-derived material. Nonetheless, other possible sources of FDOM must be considered. Besides phytoplankton activity, bacterial production (Boyd and Osburn, 2002; Cammack et al., 2004) and riverine discharge and/or watershed runoff of lignin-phenols from vascular plants are also sources of peak T (Maie et al., 2007).

BB-DOM also displayed features distinct from those of *Microcystis*-DOM. A greater content of CDOM ($a254$ and $SUVA_{254}$), more CHO-only formulae and the stronger signal of peaks M and C + A (Table 1 and 2, Figs. 3 and 4), for example, suggest the influence of terrigenous
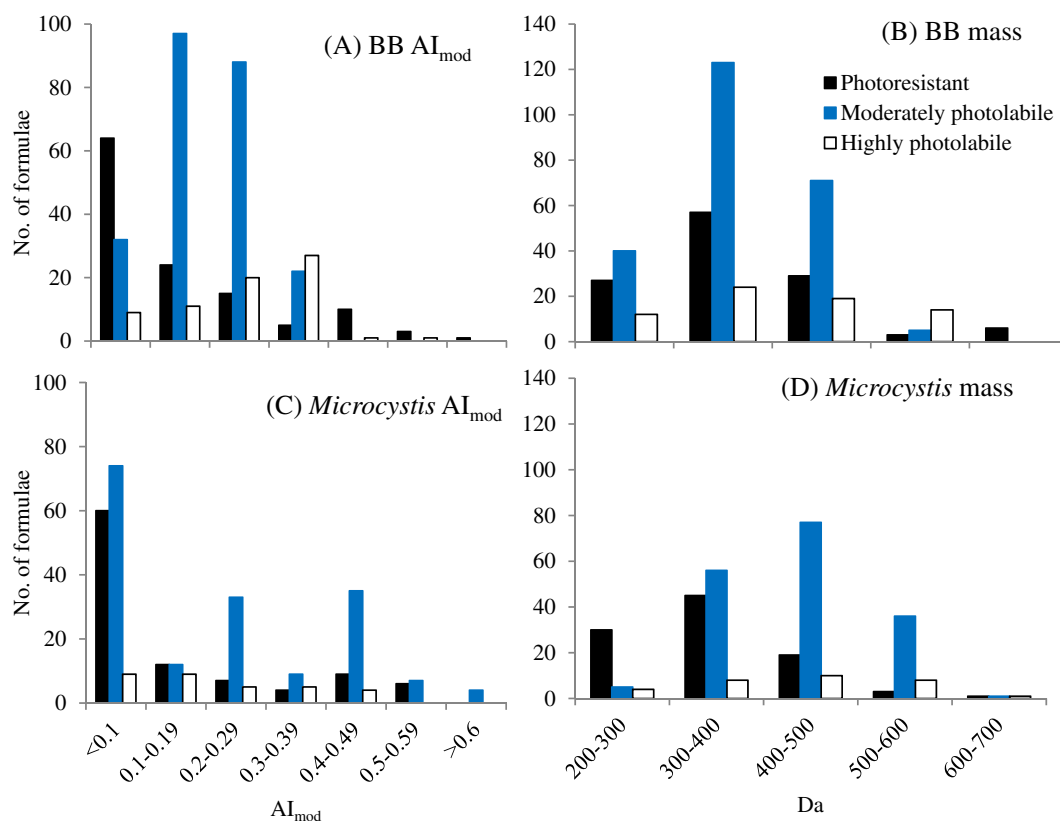
**Fig. 6.** Frequency of distribution of number of formulae classified as photoresistant (black bars), moderately photolabile (blue bars) and highly photolabile (white bars) in each range interval (bin) of modified aromaticity index ($AI_{mod}$) (A, C) and molecular mass (Da) (B, D) for BB-DOM (A, B) and *Microcystis*-DOM (C, D).

humic material input (Coble, 1996, Minor et al., 2012), runoff from the agricultural surroundings (Borisover et al., 2009) and byproducts of microbial respiration (Coble, 1996) as potential sources of DOM in the reservoir. Another clear distinction between these types of DOM was the higher relative contribution of moderately unsaturated structures in BB-DOM versus a high relative content of peptide-like formulae in *Microcystis*-DOM (Table 2). Moderately unsaturated formulae can represent multiple biogeochemically distinct structural isomers, including carboxylic-rich alicyclic molecules (CRAM) (Hertkorn et al., 2006) and lignin (Dittmar and Stubbins, 2014; Sleighter and Hatcher, 2008; Stubbins et al., 2010), which is unique to vascular plants and thus used as a tracer of terrigenous DOM (Hedges and Mann, 1979; Hernes and Benner, 2006; Spencer et al., 2009). Either microbial reworking of phytoplankton DOM that results in formation of CRAM (Hertkorn et al., 2006), or riverine and runoff inputs of terrigenous DOM could be sources of moderately unsaturated structures in the reservoir. Both CRAM and lignin-like material are considered less biolabile than freshly produced phytoplankton DOM (Hertkorn et al., 2006; Ward et al., 2013) and thus are more likely to accumulate over time in the reservoir than peptides/proteins from phytoplankton, which are more biolabile (Benner and Kaiser, 2011).

### 4.2. Photodegradation

In spite of similar DOC decay rates, qualitative photo-alteration (e.g., loss of CDOM and total molecular formulae) of BB-DOM was more pronounced than for *Microcystis*-DOM. Decay of FDOM components also differed between BB- and *Microcystis* DOM, likely due to distinct starting compositions. For instance, peak T is likely comprised of protein-like material in *Microcystis*-DOM, but could be a mixture of protein- and lignin-like moieties in BB-DOM (Maie et al., 2007). The decay rates of FDOM components are also likely influenced by

simultaneous underlying photoproduction of FDOM, particularly peaks C + A and peak M (Helms et al., 2014; Ishii and Boyer, 2012).

The decreases in CDOM absorbance, $SUVA_{254}$ values (Figs. 2 and 3), DOC-normalized FDOM, and $AI_{mod}$ (Table 2, Fig. 4) suggested that photodegradation caused loss of aromatic, potentially terrestrial signatures, transforming BB-DOM into a more aliphatic-rich DOM pool, which is in agreement with previous reports (Helms et al., 2014; Sleighter and Hatcher, 2008; Stubbins et al., 2010). These results suggest that photodegradation has the potential to mask the allochthonous-DOM signature and overestimate the *Microcystis*-DOM signature in BB-DOM at the surface layer of the reservoir, given the typical water column stability of this water body and high insolation throughout the year.

Photoproducts comprised a minor portion of the photodegraded samples, in agreement with previous studies (Stubbins et al., 2010). While photoproduct are described here and in previous photochemistry studies (Stubbins et al., 2010; Rossel et al., 2013), the unequivocal identification of 'new' formulae can be complicated by shifts in charge competition in the FTICR-MS ionization source due to photodegradation. Such shifts could have resulted in some molecules present in initial samples increasing in abundance (i.e., with higher S/N) in the mass spectra for the photodegraded sample due to the loss of DOC and a probable accompanying loss of the total number of molecules competing for charge. For *Microcystis*-DOM, photodegradation resulted in reduced molecular size, as suggested by blue-shifts of CDOM peaks (Fig. 2C) (Helms et al., 2008, 2013; Pavia et al., 1979) and the decrease in median of molecular mass (Da) detected by FTICR-MS (Table 2, Fig. 6D). Photodegradation affected the elemental composition of BB- and *Microcystis*-DOM in different ways (Table 2), with preferential removal of CHO-only formulae and moderately unsaturated compounds, potentially representative of lignin-phenols, in BB-DOM (Rossel et al., 2013; Stubbins et al., 2010), and preferential removal of CHO + N in *Microcystis*-DOM (Bittar et al.,

2015). These results indicate that photodegradation has the potential to reduce the overall degree of molecular conjugation, size and N content of autochthonous DOM in high primary productivity waters. Such transformations have implications to downstream processes such as biological utilization of this less aromatic, lower molecular mass and N-depleted pool of DOM.

### 4.3. Effects of photodegradation on the similarity between BB-DOM and Microcystis-DOM

In spite of potential differences between DOM from lab-cultured and natural populations of *Microcystis*, the *Microcystis*-DOM examined in this study represents 'pure' phytoplankton-derived DOM, i.e., that has not undergone any degree of photochemical or bacterial degradation prior to the UVB experiments. Since the reservoir is continuously exposed to sunlight, BB-DOM has unequivocally undergone a degree of photodegradation prior to our sampling. Thus, we hypothesized that BB-DOM at the time of sampling (0 d) would more likely contain photodegraded *Microcystis*-DOM than unaltered *Microcystis*-DOM. If that was the case, the FTICR-MS profile of initial BB-DOM (0 d) would be more similar to the photodegraded *Microcystis*-DOM (0.5 d and 7 d) than to non-degraded *Microcystis*-DOM (0 d). This trend was observed to a certain extent, as photodegraded *Microcystis*-DOM became more similar to BB-DOM at 0 d, with similarity indexes increasing from 0.16 to 0.18 at 0.5 d and to 0.24 at 7 d of exposure to UVB (Table 3). FTICR-MS analyses were not run in replicates, so the statistical significance of these JSI could not be assessed. At the same time, increasing similarity was observed between photodegraded BB-DOM (0.5 d and 7 d) and the non-irradiated *Microcystis*-DOM (0 d) (from 0.16 to 0.17 at 0.5 d, and to 0.23 at 7 d; Table 3). One could argue that photoreactivity of *Microcystis*-DOM was theoretically lower compared to photoreactivity of the terrigenous fraction of BB-DOM and, consequently, photodegraded BB-DOM lost its terrigenous features, becoming more similar to *Microcystis*-DOM (0 d). While similarity increased over time of UVB exposure in both directions (i.e., photodegraded BB-DOM was more similar to unaltered *Microcystis*-DOM and vice versa, Table 3), the similarity index between the two 7 d-photodegraded samples was 0.59, ~3-fold greater than the JSI of any other sample pair (Table 3). These results suggest that (1) BB-DOM is not 'simply' composed of photodegraded *Microcystis*-DOM, but by a more complex mixture of sources, and that (2) *Microcystis*-DOM, despite low aromaticity, is not photochemically inert. Most notably, observation of the highest JSI for BB- and *Microcystis*-DOM after 7 d of irradiation indicates that photodegradation increases the similarities between samples by decreasing the chemical diversity of DOM through the selective removal and production of chemically defined suites of molecules (Stubbins et al., 2010; Kellerman et al., 2014).

### 4.4. Final considerations

This study showed that DOM from the tropical eutrophic Barra Bonita Reservoir is likely influenced by autochthonous sources, such as *Microcystis* exudation, and that photodegradation has the potential to alter not only the optical and chemical properties of BB-DOM, but also those of "pure" phytoplankton DOM. Significantly more quantitative field data for light attenuation and for the apparent quantum yield spectra of reactions need to be experimentally determined (i.e., a wavelength dependent photon-by-photon accounting is required) in order to extrapolate these laboratory data on photochemical rates to the water column. The euphotic zone for primary production in the Barra Bonita Reservoir varies from 1 to ~12 m throughout the year (Dellamano-Oliveira et al., 2008), but due to high concentrations of CDOM, UVB radiation in the Barra Bonita Reservoir likely penetrates only the first few centimeters of the surface layer. While this represents a minor portion of the water column, DOM across the whole reservoir area of 325 km$^2$ is subject to photodegradation by UVB year-round.

Due to water column stability and *Microcystis* buoyancy regulation capability, phytoplankton blooms dominated by this species typically remain at the water surface for days to weeks. Given that bacterial abundance and activity tend to be low at the water surface (Vieira et al., 2013), and that phytoplankton release of DOM is generally greater during daylight hours (Kaplan and Bott, 1982), UVB degradation of *Microcystis*-derived DOM could be a significant mechanism of DOM removal and transformation at the surface of the reservoir. Photodegradation of DOM is considered an important process of C cycling in temperate lakes, including those where the autochthonous DOM component is equally or more dominant relative to terrigenous sources (Bertilsson and Tranvik, 2000; Kellerman et al., 2014; Minor et al., 2012), and this study extends the potential relevance of this process into tropical lakes.

### Appendix A. Supplementary data

Supplementary data associated with this article can be found in the online version, at http://dx.doi.org/10.1016/j.marchem.2015.06.016. These data include the Google map of the most important areas described in this article.

### References

Anesio, A.M., Granéli, W., 2003. Increased photoreactivity of DOC by acidification: implication for carbon cycle in humic lakes. Limnol. Oceanogr. 48, 735–744.

Aufdenkampe, A.K., Mayorga, E., Raymond, P.A., Melack, J., Doney, S.C., Alin, S.R., Aalto, R.E., Yoo, K., 2011. Riverine coupling of biogeochemical cycles between land, oceans, and atmosphere. Front. Ecol. Environ. 9, 53–60.

Battin, T.J., Luyssaert, S., Kaplan, L.A., Aufdenkampe, A.K., Richter, A., Tranvik, L.J., 2009. The boundless carbon cycle. Nat. Geosci. 2, 598–600.

Benner, R., Kaiser, K., 2011. Biological and photochemical transformations of amino acids and lignin phenols in riverine dissolved organic matter. Biogeochemistry 102, 209–222.

Bertilsson, S., Tranvik, L.J., 2000. Photochemical transformation of dissolved organic matter in lakes. Limnol. Oceanogr. 49, 753–762.

Bittar, T.B., Vieira, A.A.H., Stubbins, A., Mopper, K., 2015. Competition between photochemical and biological degradation of dissolved organic matter from the cyanobacteria *Microcystis aeruginosa*. Limnol. Oceanogr. http://dx.doi.org/10.1002/lno.10090.

Boreen, A.L., Edhlund, B.L., Cotner, J.B., McNeill, K., 2008. Indirect photodegradation of dissolved free amino acids: the contribution of singlet oxygen and the differential reactivity of DOM from various sources. Environ. Sci. Technol. 42, 5492–5498.

Borisover, M., Laor, Y., Parparov, A., Bukhanovsky, N., Lado, M., 2009. Spatial and seasonal patterns of fluorescent organic matter in lake Kinneret (Sea of Galilee) and its catchment basin. Water Res. 43, 3104–3116.

Boyd, T.J., Osburn, C.L., 2002. Changes in CDOM Fluorescence From Allochthonous and Autochthonous Sources During Tidal Mixing and Bacterial Degradation in Two Coastal Estuaries, Ocean Sciences Meeting 2002. Elsevier, Honolulu, pp. 189–210.

Brookes, J.D., Granf, G.G., 2001. Variations in the buoyancy response of *Microcystis aeruginosa* to nitrogen, phosphorus and light. J. Plankton Res. 23, 1399–1411.

Calijuri, M.C., Dos Santos, A.C.A., Jati, S., 2002. Temporal changes in the phytoplankton community structure in a tropical and eutrophic reservoir (Barra Bonita, S.P., Brazil). J. Plankton Res. 24, 617–634.

Cammack, W.K.L., Kalff, J., Prairie, Y.T., Smith, E.M., 2004. Fluorescent dissolved organic matter in lakes: relationships with heterotrophic metabolism. Limnol. Oceanogr. 49, 2034–2045.

Chen, H., Stubbins, A., Hatcher, P.G., 2011. A mini-electrodialysis system for desalting small volume saline samples for Fourier transform ion cyclotron resonance mass spectrometry. Limnol. Oceanogr. Methods 9, 582–592.

Coble, P.G., 1996. Characterization of marine and terrestrial DOM in seawater using excitation–emission matrix spectroscopy. Mar. Chem. 51, 325–346.

Cole, J.J., Prairie, Y.T., Caraco, N.F., McDowell, W.H., Tranvik, L.J., Striegl, R.G., Duarte, C.M., Kortelainen, P., Downing, J.A., Middelburg, J.J., Melack, J., 2007. Plumbing the global

carbon cycle: integrating inland waters into the terrestrial carbon budget. Ecosystems 10, 171–184.

Cory, R.M., McKnight, D.M., Chin, Y.-P., Miller, P., Jaros, C.L., 2007. Chemical characteristics of fulvic acids from arctic surface waters: microbial contributions and photochemical transformations. J. Geophys. Res. 112, G04S51. http://dx.doi.org/10.1029/2006jg000343.

Cory, R., Miller, M.P., McKnight, D.M., Guerard, J.J., Miller, P.L., 2010. Effect of instrument-specific response on the analysis of fulvic acid fluorescence spectra. Limnol. Oceanogr. Methods 8, 67–78.

Dellamano-Oliveira, M.J., Vieira, A.A.H., Rocha, O., Colombo-Corbi, V., Sant'anna, C.L., 2008. Phytoplankton taxonomic composition and temporal changes in a tropical reservoir. Fundam. Appl. Limnol. 171, 27–38.

Dittmar, T., Stubbins, A., 2014. Dissolved organic matter in aquatic systems. In: Birrer, B., Falkowski, P., Freeman, K. (Eds.), Treatise of Geochemistry. Elsevier, pp. 125–156.

Fellman, J.B., Hood, E., Spencer, R.G.M., 2010. Fluorescence spectroscopy opens new windows into dissolved organic matter dynamics in freshwater ecosystems: a review. Limnol. Oceanogr. 55, 2452–2462.

Fogg, G.E., 1983. The ecological significance of extracellular products of phytoplankton photosynthesis. Bot. Mar. 26, 3–14.

Gonsior, M., Peake, B.M., Cooper, W.T., Podgorski, D., D'andrilli, J., Cooper, W.J., 2009. Photochemically induced changes in dissolved organic matter identified by ultrahigh resolution Fourier transform ion cyclotron resonance mass spectrometry. Environ. Sci. Technol. 43, 698–703.

Gorham, P.R., McLachlan, J., Hammer, U.T., 1964. Isolation and culture of toxic strains of Anabaena flos-aquae. Breb. Int. Ver. Theor. Angew. Limnol. Verh. 19, 796–804.

Green, S.A., Blough, N.V., 1994. Optical absorption and fluorescence properties of chromophoric dissolved organic matter in natural waters. Limnol. Oceanogr. 39, 1903–1916.

Hedges, J.I., Mann, D.C., 1979. The characterization of plant tissues by their lignin oxidation products. Geochim. Cosmochim. Acta 43, 1803–1807.

Helms, J.R., Stubbins, A., Ritchie, J.D., Minor, E.C., Kieber, D.J., Mopper, K., 2008. Absorption spectral slopes and slope ratios as indicators of molecular weight, source, and photobleaching of chromophoric dissolved organic matter. Limnol. Oceanogr. 53, 955–969.

Helms, J.R., Stubbins, A., Perdue, E.M., Green, N.W., Chen, H., Mopper, K., 2013. Photochemical bleaching of oceanic dissolved organic matter and its effect on absorption spectral slope and fluorescence. Mar. Chem. 155, 81–91.

Helms, J.R., Mao, J., Stubbins, A., Schmidt-Rohr, K., Spencer, R.G.M., Hernes, P.J., Mopper, K., 2014. Loss of optical and molecular indicators of terrigenous dissolved organic matter during long-term photobleaching. Aquat. Sci. 76, 353–373.

Hernes, P.J., Benner, R., 2006. Terrigenous organic matter sources and reactivity in the North Atlantic Ocean and a comparison to the Arctic and Pacific oceans. Mar. Chem. 100, 66–79.

Hertkorn, N., Benner, R., Frommberger, M., Schmitt-Kopplin, P., Witt, M., Kaiser, K., Kettrup, A., Hedges, J.I., 2006. Characterization of a major refractory component of marine dissolved organic matter. Geochim. Cosmochim. Acta 70, 2990–3010.

Ishii, S.K., Boyer, T.H., 2012. Behavior of reoccurring PARAFAC components in fluorescent dissolved organic matter in natural and engineered systems: a critical review. Environ. Sci. Technol. 46, 2006–2017.

Jaccard, P., 1912. The distribution of the flora in the alpine zone. New Phytol. 9 (2), 37–50.

Kaplan, L.A., Bott, T.L., 1982. Diel fluctuations of DOC generated by algae in a piedmont stream. Limnol. Oceanogr. 27, 1091–1100.

Kellerman, A.M., Dittmar, T., Kothawala, D.N., Tranvik, L.J., 2014. Chemodiversity of dissolved organic matter in lakes driven by climate and hydrology. Nat. Commun. http://dx.doi.org/10.1038/ncomms4804.

Kluijver, A., Yu, J., Houtekamer, M., Middelburg, J.J., Liu, Z., 2012. Cyanobacteria as a carbon source for zooplankton in eutrophic lake Taihu, China, measured by $^{13}C$ labeling and fatty acid biomarkers. Limnol. Oceanogr. 57, 1245–1254.

Koch, B.P., Dittmar, T., 2006. From mass to structure: an aromaticity index for high-resolution mass data of natural organic matter. Rapid Commun. Mass Spectrom. 20, 926–932.

Kujawinski, E.B., 2002. Electrospray ionization Fourier transform ion cyclotron mass spectrometry (ESI-FT-ICR-MS): characterization of complex environmental mixtures. Environ. Forensic 3, 207–216.

Kujawinski, E.B., Del Vecchio, R., Blough, N.V., Klein, G.C., Marshall, A.G., 2004. Probing molecular-level transformations of dissolved organic matter: insights on photochemical degradation and protozoan modification of DOM from electrospray ionization Fourier transform ion cyclotron resonance mass spectrometry. Mar. Chem. 92, 23–37.

Lewis, W.M.J., 2000. Basis for the protection and management of tropical lakes. Lakes Reserv. Res. Manag. 5, 35–48.

Liu, Z., Hader, D.P., Sommaruga, R., 2004. Occurrence of mycosporine-like amino acids (MAAs) in the bloom-forming cyanobacterium Microcystis aeruginosa. J. Plankton Res. 26, 963–966.

Loiselle, S.A., Bracchini, L., Dattilo, A.M., Rici, M., Tognazzi, A., Cozar, A., Rossi, C., 2009. Optical characterization of chromophoric dissolved organic matter using wavelength distribution of absorption spectral slopes. Limnol. Oceanogr. 52, 590–597.

Mague, T.H., Friberg, E., Hughes, D.J., Morris, I., 1980. Extracellular release of carbon by marine phytoplankton: a physiological approach. Limnol. Oceanogr. 25, 262–279.

Maie, N., Scully, N.M., Pisani, O., Jaffe, R., 2007. Composition of a protein-like fluorophore of dissolved organic matter in coastal wetland and estuarine ecosystems. Water Res. 41, 563–570.

McLafferty, F.W., Turecek, F., 1993. Interpretation of Mass Spectra. University Science Books, Mill Valley, California, USA.

Minor, E.C., Dalzell, B.J., Stubbins, A., Mopper, K., 2007. Evaluating the photoalteration of estuarine dissolved organic matter using direct temperature-resolved mass spectrometry and UV–visible spectroscopy. Aquat. Sci. 69, 440–455.

Minor, E.C., Steinbring, C.J., Longnecker, K., Kujawinski, E.B., 2012. Characterization of dissolved organic matter in Lake Superior and its watershed using ultrahigh resolution mass spectrometry. Org. Geochem. 43, 1–11.

Mopper, K., Zhou, X., Kieber, R.J., Kieber, D.J., Sikorski, R.J., Jones, R.D., 1991. Photochemical degradation of dissolved organic carbon and its impact on the oceanic carbon cycle. Science 353, 60–62.

Mopper, K., Kieber, D.J., Stubbins, A., 2015. Marine photochemistry of organic matter: processes and impacts. In: Hansell, D.A., Carlson, C.A. (Eds.), Marine Photochemistry of Organic Matter. Elsevier, pp. 389–450.

Moran, M.A., Zepp, R.G., 1997. Role of photoreactions in the formation of biologically labile compounds from dissolved organic matter. Limnol. Oceanogr. 42, 1307–1316.

Moran, M.A., Sheldon, W.M.J., Zepp, R.G., 2000. Carbon loss and optical property changes during long-term photochemical and biological degradation of estuarine dissolved organic matter. Limnol. Oceanogr. 45, 1254–1264.

Paerl, H.W., Huisman, J., 2008. Blooms like it hot. Science 320, 57–58.

Paerl, H.W., Otten, T.G., 2013. Blooms bite the hand that feeds them. Science 342, 433–434.

Pavia, D.L., Lampan, G.M., Kriz, G.S., 1979. Introduction to Spectroscopy: A Guide for Students of Organic Chemistry. Saunders.

Rossel, P.E., Vähätalo, A.V., Witt, M., Dittmar, T., 2013. Molecular composition of dissolved organic matter from a wetland plant (Juncus effusus) after photochemical and microbial decomposition (1.25 yr): common features with deep sea dissolved organic matter. Org. Geochem. 60, 62–71.

Sivonen, K., Jones, G.J., 1999. Cyanobacteria toxins. In: Chorus, Bartman, J. (Eds.), Toxic cyanobacteria in water. E & FN Spon., pp. 41–111.

Sleighter, R.L., Hatcher, P.G., 2008. Molecular characterization of dissolved organic matter (DOM) along a river to ocean transect of the lower Chesapeake Bay by ultrahigh resolution electrospray ionization Fourier transform ion cyclotron resonance mass spectrometry. Mar. Chem. 110, 140–152.

Sleighter, R.L., McKee, G., Liu, Z., Hatcher, P.G., 2008. Naturally present fatty acids as internal calibrants for Fourier transform mass spectra of dissolved organic matter. Limnol. Oceanogr. Methods 6, 246–253.

Spencer, R.G., Baker, A., Ahad, J.M., Cowie, G.L., Ganeshram, R., Upstill-Goddard, R.C., Uher, G., 2007. Discriminatory classification of natural and anthropogenic waters in two U.K. Estuaries. Sci. Total Environ. 373, 305–323.

Spencer, R.G.M., Stubbins, A., Hernes, P.J., Baker, A., Mopper, K., Aufdenkampe, A.K., Dyda, R.Y., Mwamba, V.L., Mangangu, A.M., Wabakanghanzi, J.N., Six, J., 2009. Photochemical degradation of dissolved organic matter and dissolved lignin phenols from the congo river. J. Geophys. Res. 114, G03010. http://dx.doi.org/10.1029/2009jg000968.

Spencer, R.G.M., Guo, W., Raymond, P.A., Dittmar, T., Hood, E., Fellman, J., Stubbins, A., 2014. Source and biolability of ancient dissolved organic matter in glacier and lake ecosystems on the Tibetan plateau. Geochim. Cosmochim. Acta 142, 64–74.

Stedmon, C.A., Bro, R., 2008. Characterizing dissolved organic matter fluorescence with parallel factor analysis: a tutorial. Limnol. Oceanogr. Methods 6, 572–579.

Stedmon, C.A., Markager, S., 2005. Tracing the production and degradation of autochthonous fractions of dissolved organic matter by fluorescence analysis. Limnol. Oceanogr. 50, 1415–1426.

Stubbins, A., Dittmar, T., 2012. Low volume quantification of dissolved organic carbon and dissolved nitrogen. Limnol. Oceanogr. Methods 10, 347–352.

Stubbins, A., Spencer, R.G.M., Chen, H.M., Hatcher, P.G., Mopper, K., Hernes, P.J., Mwamba, V.L., Mangangu, A.M., Wabakanghanzi, J.N., Six, J., 2010. Illuminated darkness: molecular signatures of Congo River dissolved organic matter and its photochemical alteration as revealed by ultrahigh precision mass spectrometry. Limnol. Oceanogr. 55, 1467–1477.

Stubbins, A., Law, C.S., Uher, G., Upstill-Goddard, R.C., 2011. Carbon monoxide apparent quantum yields and photoproduction in the Tyne Estuary. Biogeosciences 8, 703–713.

Stubbins, A., Niggemann, J., Dittmar, T., 2012. Photo-lability of deep ocean dissolved black carbon. Biogeosciences 9, 1661–1670.

Stubbins, A., Lapierre, J.F., Berggren, M., Prairie, Y., Dittmar, T., Del Giorgio, P.A., 2014. What's in an EEM? Molecular signatures associated with dissolved organic fluorescence in boreal Canada. Environ. Sci. Technol. 48, 10598–10606.

Tien, C.J., Krivtsov, V., Levado, E., Sigee, D.C., White, K.N., 2002. Occurrence of cell-associated mucilage and soluble extracellular polysaccharides in Rostherne Mere and their possible significance. Hydrobiologia 485, 245–252.

Tranvik, L.J., Bertilsson, S., 2001. Contrasting effects of solar UV radiation on dissolved organic sources for bacterial growth. Ecol. Lett. 4, 458–463.

Tranvik, L.J., Olofsson, H., Bertilsson, S., 2000. Photochemical effects on bacterial degradation of dissolved organic matter in lake water. In: Bell, C.R., Brylinsky, M., Johnson-Green, P.C. (Eds.), Microbial Biosystems: New Frontiers. Proc. 8th Int. Symp. Microb. Ecol., Halifax, Canada, pp. 193–200.

Tundisi, J.G., Matsumura-Tundisi, T., Abe, D.S., 2008. The ecological dynamics of Barra Bonita (Tietê River, S.P., Brazil) Reservoir: implications for its biodiversity. Braz. J. Biol. 68, 1079–1098.

Vieira, A.A.H., Ortolano, P.H.C., Giroldo, D., Dellamano-Oliveira, M.J., Bittar, T.B., Lombardi, A.T., Sartori, A.L., Paulsen, B.S., 2008. Role of hydrophobic extracellular polysaccharide of Aulacoseira granulata (Bacillariophyceae) on aggregate formation in a turbulent and hypereutrophic reservoir. Limnol. Oceanogr. 53, 1887–1899.

Vieira, A.A.H., Colombo-Corbi, V., Bagatini, I.L., Dellamano-Oliveira, M.J., Tessarolli, L.P., 2013. Rhamnose and hydrolysis of muf-α-L-rhamnopyranoside coupled with producers of rhamnose-rich extracellular polysaccharides in a hypereutrophic reservoir. Aquat. Microb. Ecol. 69, 169–181.

Vodacek, A., Blough, N.V., DeGrandpre, M.D., Peltzer, E.T., Nelson, R.K., 1997. Seasonal variation of CDOM and DOC in the Middle Atlantic Bight: terrestrial inputs and photooxidation. Limnol. Oceanogr. 42, 674–686.

Walsh, J.J., Weisberg, R.H., Dieterle, D.A., He, R., Darrow, B.P., Jolliff, J.K., Lester, K.M., Vargo, G.A., Kirkpatrick, G.J., Fanning, K.A., Sutton, T.T., Jochens, A.E., Biggs, D.C., Nababan, B., Hu, C., Muller-Karger, F.E., 2003. Phytoplankton response to intrusions of slope water on the West Florida Shelf: models and observations. J. Geophys. Res. 108 (C6), 3190. http://dx.doi.org/10.1029/2002JC001406.

Ward, N.D., Keil, R.G., Medeiros, P.M., Brito, D.C., Cunha, A.C., Dittmar, T., Yager, P.L., Krusche, A.V., Richey, J.E., 2013. Degradation of terrestrially derived macromolecules in the Amazon River. Nat. Geosci. 6, 530–533.

Weishaar, J.L., Aiken, G., Bergamaschi, B.A., Fram, M.S., Fujii, R., Mopper, K., 2003. Evaluation of specific ultraviolet absorbance as an indicator of the chemical composition and reactivity of dissolved organic carbon. Environ. Sci. Technol. 37, 4702–4708.

Welch, E.B., Lindell, T., 1992. Ecological Effects of Wastewater: Applied Limnology and Pollution Effects. E & FN Spon, London.

Williamson, C.E., Morris, D.P., Pace, M.L., Olson, O.G., 1999. Dissolved organic carbon and nutrients as regulators of lake ecosystems: resurrection of a more integrated paradigm. Limnol. Oceanogr. 44, 795–803.